JOURNAL OF MATERIALS SCIENCE 26 (1991) 6035–6043

Packing of bimodal mixtures of colloidal silica

F. G. R. GAUTHIER
Reegie National des Usines Renault, Ceramiques et Plastiques Mechaniques, 92109 Boulogne Billancourt Cedex, Paris, France

S. C. DANFORTH
Center for Ceramics Research, Department of Ceramic Engineering, Rutgers University, Piscataway, NJ 08855, USA

The aim of this work was to determine the influence of the size distribution of silica powders on the characteristics of the resultant green bodies obtained by colloidal filtration. In order properly to investigate the scientific relationships between the forming parameters and the nature of the particle packing, a model ceramic material was chosen, i.e. monosized (100 and 10 nm) spherical powders of SiO_2 and colloidal filtration under 3.45 MPa was used to cast monomodal and bimodal mixtures of silica sols. The electrophoretic and rheological behaviour of those systems have been investigated. The permeability as well as the pore size distribution was found to decrease as the volume faction of fines increased (to 30%). The evolution of the density as a function of the volume fraction of fines follows the behaviour observed for the packing of bimodal mixtures of hard spheres. The systems with only one size particle were found to pack with densities close to that of random close packing. Two dimensional computer simulations and correlation to the experimental results showed that a model of "triangular" pores is preferred to a model of "square" pores.

1. Introduction

1.1. Pore structure

The main advantage of the slip casting process is its ability to form complex shapes with uniform, agglomerate free microstructures. The major disadvantage is that dimensional control is poor due to a number of factors, namely particle packing heterogeneities and shrinkages occurring during drying and sintering. The particle packing, in turn, depends on the slip viscosity, water content, mould and powder properties [1]. The density of the casting, which will have a large influence on the drying and sintering shrinkage, is dependent upon a number of factors; among them, the particle size distribution of the powder, the state of agglomeration and the packing efficiency [2].

In addition to the emphasis put on particle packing, it is also critical to evaluate the nature of the pore structure in the green body. The pore coordination number, R, is defined as the number of particles which surround and define the pore surface, and determines whether or not the pore can eventually disappear by mass transport [3]. In general, for a given dihedral angle, ϕ, there exists a critical coordination number, R_c. Pores with a coordination number lower than R_c will disappear during sintering [4]. Pores with a higher coordination number will shrink to an equilibrium size, becoming thermodynamically stable, and thus will limit the end point density to less than theoretical [5]. The only way for these pores to be eliminated is if there is sufficient grain growth such that R becomes less than R_c. Clearly for structural applications requiring a small and narrow final grain size distribution, such grain growth is undesirable.

It has also been shown that the defects generated during the forming process (such as agglomerates), which produce large pores with large R values ($> R_c$) are responsible for microstructural non-uniformity, which can be amplified during the drying and sintering steps. This often leads to ceramic products which have lowered mechanical strengths and poor reliability [6]. In order to improve the properties and reliability of the final product, one must improve the microstructure and microstructural uniformity of the green body. This includes both particle packing and pore uniformity.

The properties of an idealized sinterable powder for producing a theoretically dense single phase ceramic are believed to be a fine size (between 0.1 and 1 μm), a narrow size distribution, an equiaxed shape, and freedom from agglomeration [7]. Techniques for synthesizing such powders have been established by many investigators [8–17].

Because the sintering rate increases with the particle coordination number, lower temperatures are required for sintering ordered arrays than disordered arrays [18]. These considerations have led to the proposal [19] that a perfect close-packed arrangement of monodispersed particles is the ideal starting point for obtaining the highest strength and reliability at the lowest cost. Such uniform microstructures can be obtained through colloidal processing of monosized spherical particles. There is some concern, however, as

0022–2461/91 $03.00 + .12

to the influence on mechanical properties of certain "ordered packing" defect structures, such as domain (grain) boundaries, etc., as shown in Fig. 1. As stated in a recent review, it is questionable whether perfect single crystal structures can be formed on a macroscopic scale [20].

1.2. Particle packing

A different approach has been to avoid particle ordering altogether and seek a random close-packed structure of narrow size distribution powder which would yield a minimum defect population. With this approach, recent results have shown significant increases in the modulus of rupture (MOR) for reaction-bonded Si_3N_4 (RBSN), made from laser-synthesized and colloidally processed silicon powders [21]. Average MOR values of 531 MPa were obtained (at 76% ρTh) in contrast to values of 276–299 MPa [22, 23] for conventionally synthesized RBSN.

Another possible approach has followed the premise that the proper solution is a controlled disorder, i.e. ideal, uniform, random close packing of bimodal or trimodal suspensions, rather than use of a single size particle [24].

1.3. Bimodal size distributions

While a recent study on the effect of particle sizes in bimodal suspensions was only carried out in two dimensions, the main conclusions may have significant relevance to three dimensional powder packing [25]. It has been shown that binary mixtures of spherical particles lead to structures with dense random packing with a smaller defect size than for monosized powders. Even though the random packing has a lower bulk density than the perfect crystalline packing, the random packing is expected to have more uniform sintering characteristics due to smaller density fluctuations in the structure. They found that if the size difference between the large and small particles was too large, particle segregation occurred, resulting in the formation of ordered domains. It is critical to carefully control the following parameters: size ratios, relative concentrations of small versus large particles and, also, the relative mobilities of the two particle sizes.

The purpose of the present study was to determine what kind of particle packing would result when using colloidal filtration of bimodal suspensions as the processing method. Based on the behaviour of larger sized powders, it was thought that the interstices of the large particles could theoretically be filled by the small particles. This would result in a reduction in the pore size as well as an increase in the density of the green body. The size ratio between the coarse and fine powders was chosen at 10, based on the work of McGeary [26]. According to the results of experiments reported by McGeary and others [27–29], the maximum green packing density for spherical steel shot was obtained using several (three or four) different particle sizes where the ratio of large to small was greater than seven. This value of seven corresponds to the triangular pore path formed by any three close-packed spheres of equal size. The packing efficiency was a maximum with a particle size ratio of ~ 10.

The silica sols used in this study were characterized from a colloidal and rheological standpoint. The rate of build-up of resultant cakes was measured. The pore size distribution, as well as the density of the cakes was also measured. The data have been used in an attempt to understand whether an ordered or a disordered microstructure could evolve from such a process. An attempt was made to determine what advantages the fine bimodal particle size distribution could bring to the characteristics of the cakes (as opposed to a fine monosized powder) in terms of packing, density, pore size, and pore size distribution.

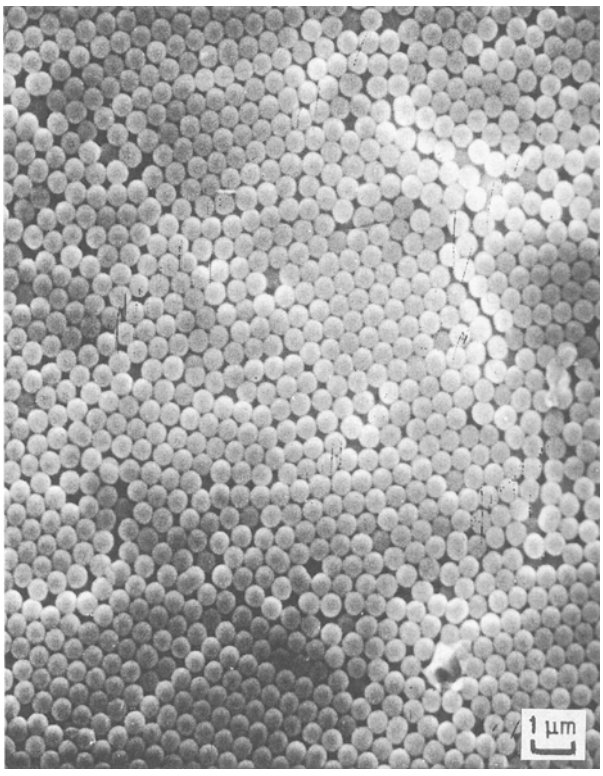

Figure 1 Scanning electron micrographs showing defects associated with crystalline or ordered particle packing.

2. Experimental procedure

2.1. Powders

In order to attain the goals outlined above, two batches of monodispersed silica particles of 10 and 100 nm were used. Table I gives the physical characteristics of the powders (Nyacol Products, Inc.,

TABLE I SiO_2 powder suspension characteristics

	Grade 830	Grade 9950
Particle size (nm)	10	100
SiO_2 (wt %)	30	50
Na_2O (wt %)	55	12
Specific gravity	1.22	1.40
pH	10.5	9.0
Viscosity (mPas)	8	18

Ashland, MA) used. The silica sols selected not only provided the proper size ratio of 10 but were also well dispersed and stable. It was not possible, however, to concentrate the sols without causing an irreversible transformation to a gel, but dilution was possible. In order to make mixtures of the two sols and to be able to make comparisons, there was a limit to the maximum solids loading of 30 wt % SiO_2. Consequently, all experiments were performed with a total solids loading of 30 wt % SiO_2 (~ 16 vol %).

Powders for characterization studies were prepared by the addition of 100 cm^3 alcohol, which led to the precipitation of the sol into a solid mass. Upon drying at 80 °C, this resulted in a fine powder. Any attempt at concentrating the sols led to the formation of a gel which would form a solid mass after drying. Since mixtures of the two sols were made and some were diluted by adding deionized water, one had to make sure that the variation of pH inherent to such operations would not have a significant effect on the electrophoretic mobility of the particles. For that reason, the variation of the zeta potential as a function of pH was measured. Powders for electrophoretic measurements were dispersed in a 10^{-3} M KCl solution to maintain the overall electrolyte concentration constant and the pH was adjusted with either additions of HCl or NaOH. This approach results in a constant double layer thickness in the four to ten pH range. At pH 2, however, the H^+ ions outnumber the K^+ ions by an order of magnitude. Consequently, the electrolyte concentration is no longer 10^{-3} M but 10^{-2} M for a 1:1 electrolyte. The double layer will then be strongly compressed, and will not extend into the solution as far as before. The determination of the zeta potential values as a function of pH was carried out using an automated zetameter (Malvern Inst., Worcester, MA).

2.2. Filtration

SiO_2 suspension viscosities were measured using a concentric cylinder viscometer (Haake Buchler, Saddle Brook, NJ) from 0–300 s^{-1}. The sols and different mixtures of fine and coarse sols were pressure cast using the cell illustrated in Fig. 2. The thickness of the cakes was measured through the transparent cell walls. The cakes were allowed to dry at room temperature until their translucent appearance was replaced by a white one and then stored in a dryer at 200 °C. The cakes were characterized for surface area and pore size distributions using the N_2 BET technique (Omicron Technology Corporation, Omnisorb, Berkley Heights, CA). The particulate densities were measured using He pycnometry (Micromeritics, Norcross, GA). Mercury porosimetry was used to measure pores with sizes greater than 600 nm (Micromeritics, Norcross, GA). Cake densities were calculated from BET measurements.

3. Results

3.1. Powder characterization

The measured densities for these powders were 2.18 g cm^{-3} for the 100 nm sol, and 2.19 g cm^{-3} for the 10 nm sol. These values are in good agreement with the value of 2.2 g cm^{-3} which is reported in the literature [30] for pure amorphous silica sols.

The results of the zeta potential measurements for grade 9950 are presented in Fig. 3. From this curve, several points should be noted. First, each point on this plot is an average of three different measurements, so that there is a high level of confidence in all points. The sharp increase in zeta potential at about pH 2 may, at first, be surprising. Second, the isoelectric point is at a pH of approximately 2. Third, a change of pH from 8 to 10 does not result in any significant change in the zeta potential value of this sol. The results for the grade 830 could not be obtained due to

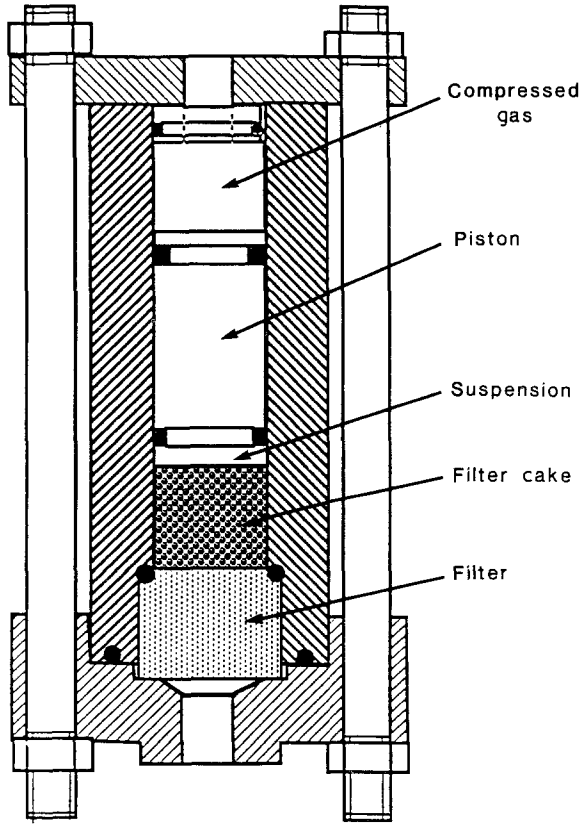

Figure 2 Schematic drawing of the transparent pressure filtration cell.

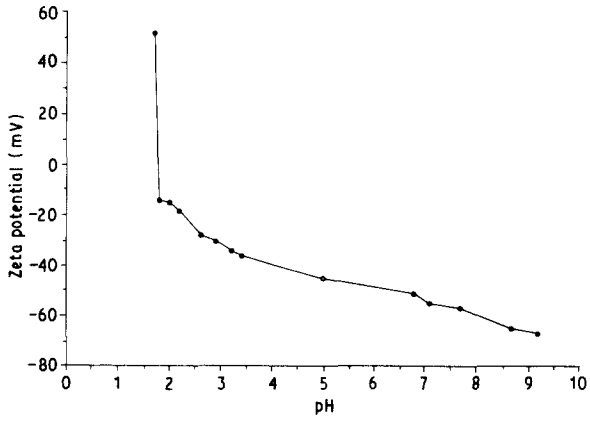

Figure 3 Zeta potential versus pH of colloidal SiO_2 powders.

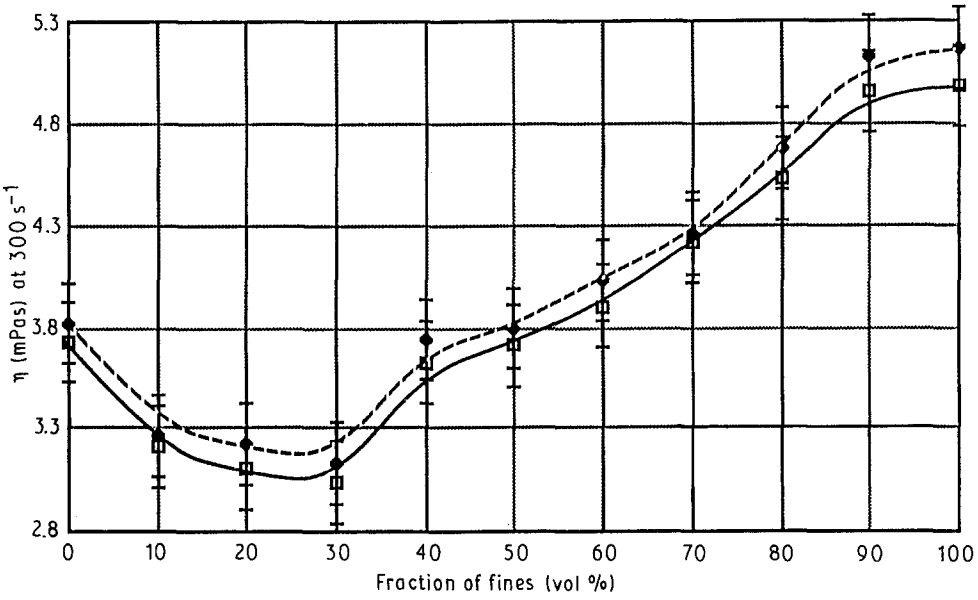

Figure 4 Viscosity (at 300 s^{-1}) versus vol % fines for bimodal SiO_2 powders. η: (□) up, (◆) down.

a very high ionic strengths which would have led to equipment damage.

Fig. 4 presents the results of the viscosity measurements at a shear rate of 300 s^{-1} as a function of the volume fraction of fines. As was true for the pure sols and for all the mixtures, the viscosity increased slightly after the samples were held at the maximum shear rate for 5 min. It can be noted that the plot is V-shaped. The viscosity goes down from 3.8 mPas for 0 vol % fines to about 3 mPas at 25 vol % fines, and then goes up to about 5 mPas for 100 vol % fines. As more and more small particles are added to the large ones, the viscosity decreases to a minimum, and after a "critical" volume fraction of fines is reached (at ~ 25–30 vol %), the viscosity increases. It should be noted that the viscosity is higher for the 10 nm particle sol than for the 100 nm particle sol.

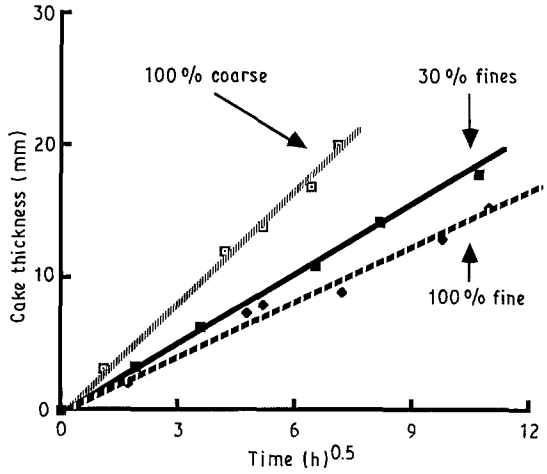

Figure 5 Cake thickness versus $t^{0.5}$ for 0, 30, and 100 vol % fines SiO_2 powder cakes.

3.2. Filtration

Fig. 5 presents a plot of the thickness of the filtered SiO_2 cakes as a function of the square root of time for 0, 30, and 100 vol % fines. The behaviour is linear, which was typical of all of the filtration experiments carried out with various sol mixtures. (It should be noted that any non-linearity at short times could not be determined using these experimental methods). It should be noted that the smaller the slope, the longer the time to build up a cake of constant thickness. The smaller slope corresponds to decreased flow through the thickness of the cake, i.e. the cake is more resistant or less permeable to the liquid flow. The slope of these plots can be related to the permeability value of the cake and the permeability and the slope both vary in the same direction.

3.2.1. Particle size distributions

In Fig. 6, the variation of the slope (of the previous type of curves), is plotted as a function of the volume fraction of the fine component in the bimodal casting suspensions. The addition of fines in the range of 0 to 100 vol % leads to a decrease in the slope of the thickness versus $t^{1/2}$ plots. If this decrease in slope is examined in the range 0–40 vol % fines, as well as in the range 60–100 vol %, a plateau or a slight increase can be noted in the range 40–60 vol % fines. The extreme values of the slope are 2.9 and 1.5 $\mu m\, h^{0.5}$ for 0 vol % fines, and 100 vol % fines, respectively (Fig. 6).

Equation 1 shows that, for the slip casting process, the thickness of the cake, L, is proportional to the square root of time, t, as [31]

$$L^2 = Pt/\{(E_{sav}/\Phi_s - 1)[1/K_{av} + (E_{sav}/\Phi_s - 1)/E_m K_m]\} = Ct \quad (1)$$

where P is the total filtration pressure (capillary pressure), E_{sav} is the volume fraction of solids in the cake, Φ_s is the volume fraction of solids in the slip, K_m is the permeability of the mould, K_{av} is the permeability of

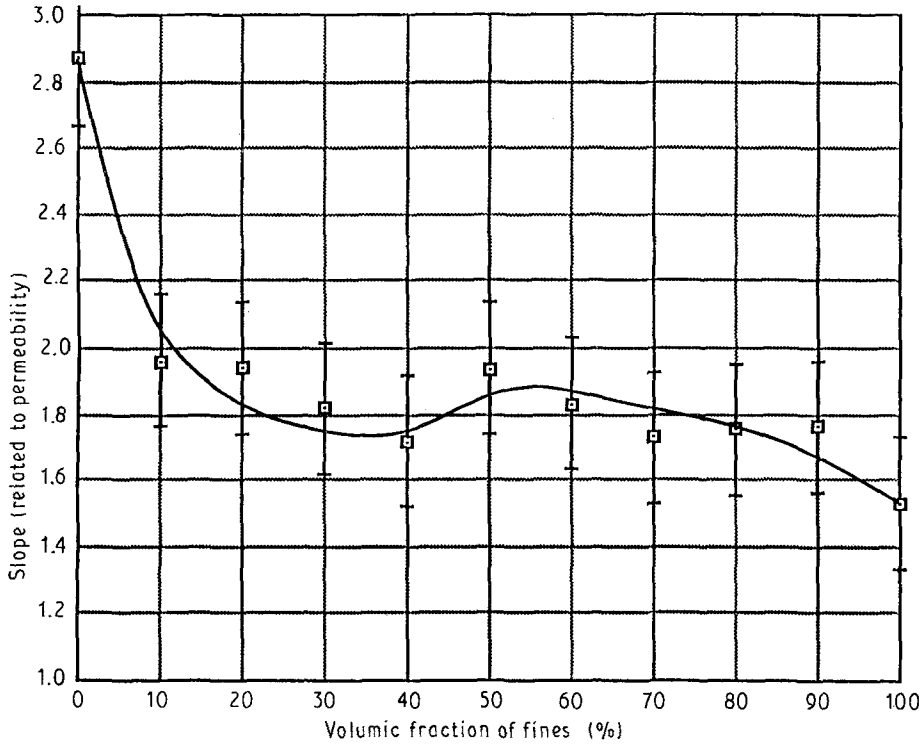

Figure 6 Slope of thickness versus $t^{0.5}$ curves for various volume fractions of fine SiO_2 powders.

the cake, E_m is the porosity of the mould, and C is a constant.

The constant, C, is a function of the volume fraction solids in the cake and in the slip and the porosity and permeability of the cake and the mould. In this case, the slope would be equal to the square root of C. Assuming that P, E_{sav}, E_m, K_m, and Φ_s defined in Equation 1 are constant during the experiment, the slope would be proportional to the square root of the average permeability of the cake. Based on these considerations, it appears that the permeability of a cake with 0 vol % fines is four times that of a cake with 100 vol % fines. It is interesting to note the very low value of the permeability at 40 vol % fines. If the evolution of the density as a function of the fine volume fraction of powders was to follow the same evolution as the system with a size ratio of 10 studied by McGeary and others [26–29], a maximum packing density would be expected between 30 and 40 vol % fines. It is reasonable to expect, therefore, that a minimum value of the permeability would correspond to the highest packing density (or the closest type of packing).

As the volume fraction of fines is increased in the range 0–50 vol %, both the average pore size and the pore size distribution width decrease as seen in Fig. 7. This is in good agreement with the fact that there is a decrease in permeability over the same range. Clearly, the cakes become less permeable as the small particles decrease the pore sizes between the large particles. The BET method is unable to detect pores above 600 nm and the results obtained detected no pores above 20 nm. Table II gives the results obtained from mercury porosimetry (SEM observations indicated that the larger pores were near the cake filter media interface), over a pressure range 15–300 p.s.i

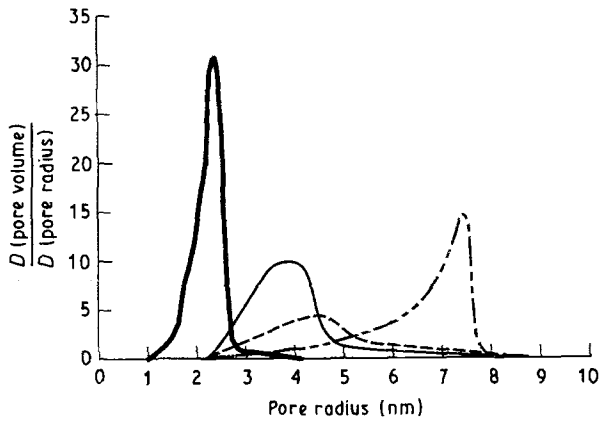

Figure 7 Pore size distributions for cakes from various mixtures of fine (10 nm) and coarse (100 nm) SiO_2 powders. (——) 100% fines, (— — —) 50% fines, (– – –) 30% fines, (– · – · –) 0% fines.

(10^3p.s.i. = 6.89 N mm^{-2}). These measurements were made in order to complete the pore size information obtained from BET. The goal was to determine if the cakes had pores larger than 600 nm. The pore volume was determined for cakes made with 0, 30, and 90 vol % fines. As can be seen from the results given in Table II, there are some pores in the cakes with sizes between 0.6 and 10 μm, but they do not contribute significantly to the total pore volume measured (0.21 and 0.24 cm^3 g^{-1}) below 0.02 μm.

Fig. 8 shows the density of the different cakes as a function of the volume fraction of fine particles. Densities were calculated from BET pore volumes and confirmed using the Archimedes method. The density is expressed as a fraction of the theoretical density (taken as 2.2 g cm^{-3}). It can be seen that the variation of the density versus the volume fraction of fines, follows a curve which reaches a maximum at about

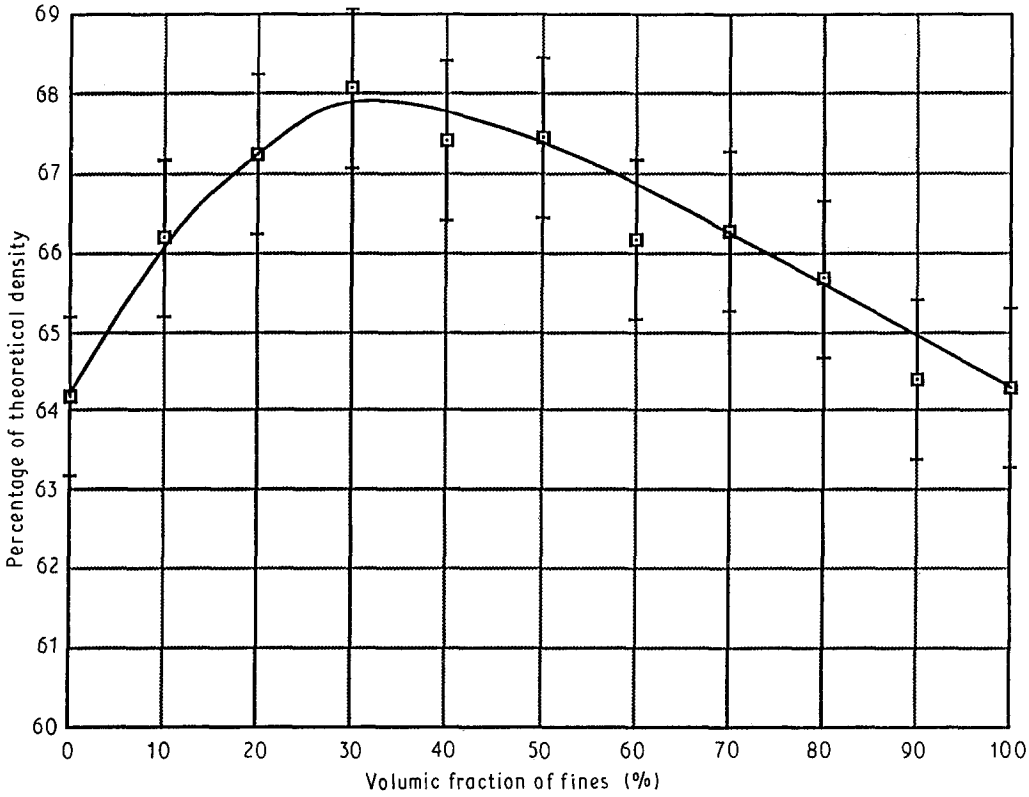

Figure 8 Density of cakes from various mixtures of fine (10 nm) and coarse (100 nm) SiO_2 powders.

TABLE II Mercury porosimetry of colloidally filtered cakes

Sample	Pore size (μm)	Pore volume (cm^3)
0 vol % fines	9.25	0.0
	3.72	0.002
	1.72	0.002
	0.96	0.002
	0.81	0.002
	0.62	0.003
	0.58	0.003
	< 0.02	0.21–0.24
30 vol % fines	9.25	0.0
	4.14	0.0
	3.03	0.00004
	1.62	0.0001
	0.64	0.0001
	0.57	0.0001
	< 0.02	0.21–0.24
90 vol % fines	9.25	0.0
	4.46	0.0001
	2.94	0.0004
	1.62	0.0004
	0.59	0.0004
	< 0.02	0.21–0.24

30 vol % fines. It should be pointed out that the maximum density obtained for 30 vol % fines is 70% theoretical while the average value at 30% fines was 68% theoretical. It should be noted that the densities at the two extremes, that is 0 and 100 vol % fines, are 64.2 and 64.3% theoretical, respectively. These values correspond closely to what has been reported for random close packing of monosized hard spheres [32].

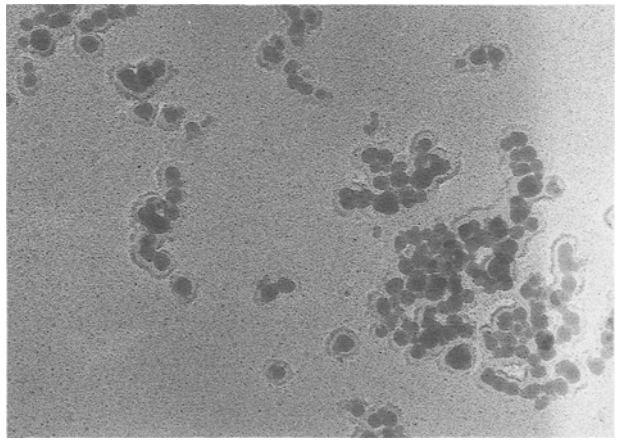

Figure 9 Transmission electron micrograph of coarse (100 nm) SiO_2 powder.

A transmission electron micrograph of the 100 nm SiO_2 powder is presented in Fig. 9. As can be seen, the particles are not quite spherical but are rather monosized and are approximately 100 nm diameter.

Fig. 10 is scanning electron micrograph of a fracture surface of a cake made with 100 vol % 100 nm particles. Some almost spherical but nonetheless discreet particles can be seen, which appear to be approximately 100 nm in size. The microstructure, although not ordered, appears to be rather densely packed with some small pores distributed rather uniformly throughout the microstructure. No large pores (in the 0.5–10 μm size range) were observed in the bulk or top surfaces of the cakes. Large pores of this size were seen at the cake filter interface. The microstructure of cakes made with 100 vol % 10 nm particles, appears to be

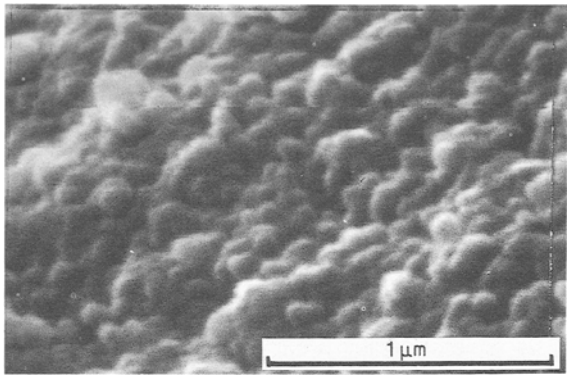

Figure 10 Scanning electron micrograph of the fracture surface of a cake made from 100% coarse (100 nm) SiO_2 powder.

densely packed with pores (~ 100 nm) distributed uniformly throughout the microstructure.

4. Discussion

4.1. Suspension characteristics

In the pH range of 4 to 10, it is certain that the zeta potentials are all measured at the same distance from the surface of the particle, and can be compared to one another. On the other hand, between pH 2 and 4, the double layer is strongly compressed since the concentration of H^+ ions becomes significant. This means that the zeta potential values obtained around pH 2 belong to a curve for an electrolyte concentration of 10^{-2} M. Nonetheless, the value of the zero point of charge should not be affected. It appears that the zero point of charge value reported for a pH of 1.95 is valid and in agreement with what is reported in the literature for pure amorphous silica.

The decrease in viscosity which was observed for different bimodal mixtures of powders is likely to be related to the concept of free volume. When small particles are added to large ones, the packing density increases until 30 vol % fines is reached, then decreases. The greater the tendency of the particles to pack efficiently, the more free liquid there will be available for flow. Thus, adding fines to the coarse powder will lower the viscosity. It can be noted that the results obtained from the viscosity measurements are in good agreement with those from the density measurements in that extremes in both cases occur at 30 vol % fines.

4.2. Pore size distribution

In order to try to relate the measured pore size distributions to some physical reality, two dimensional computer simulations were performed, in the case of four contacting spheres. The results are shown in Fig. 11 which shows four contacting spheres, each having a diameter of 100 nm. It can be seen that the equivalent diameter of the internal pore (i.e. the largest circle that will fit inside) is 41.7 nm. This calculated value, although representing an ideal case, is three times the peak pore diameter obtained from the pore size distribution curve for 100 nm particles shown in Fig. 7. It

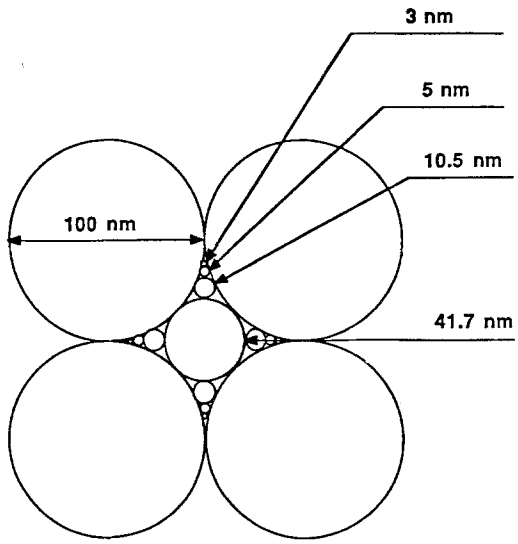

Figure 11 Two-dimensional simulation of rectangular close packing of 100 nm spheres.

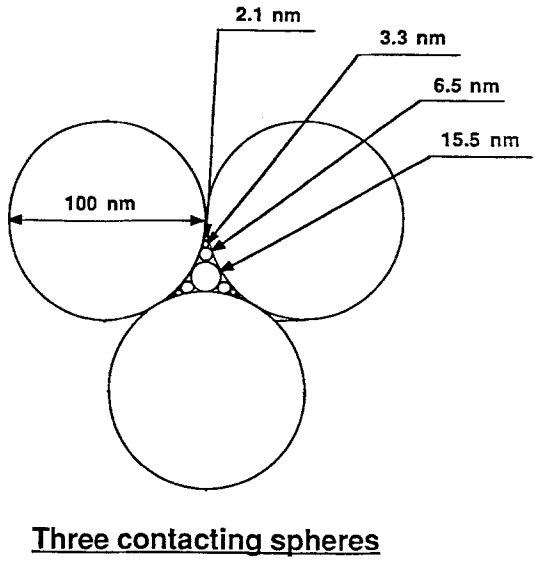

Figure 12 Two-dimensional simulation of triangular close packing of 100 nm spheres.

would seem from these considerations, that the powders are not packed with a coordination number of 4 (in two dimensions). Calculations were also made for the case where there are three contacting 100 nm spheres (in two dimensions). Those results are shown in Fig. 12. In this case, the equivalent pore diameter is 15.5 nm. This value is quite close to the result obtained from the BET experiments (15.0 nm). It would seem from these comparisons, that the four contacting spheres model can be discarded, and the three contacting sphere approximation is more representative of the actual particle packing.

In another computer simulation (Fig. 13), it was assumed that there were three contacting spheres of equal size with a 100 nm diameter. This time, it was

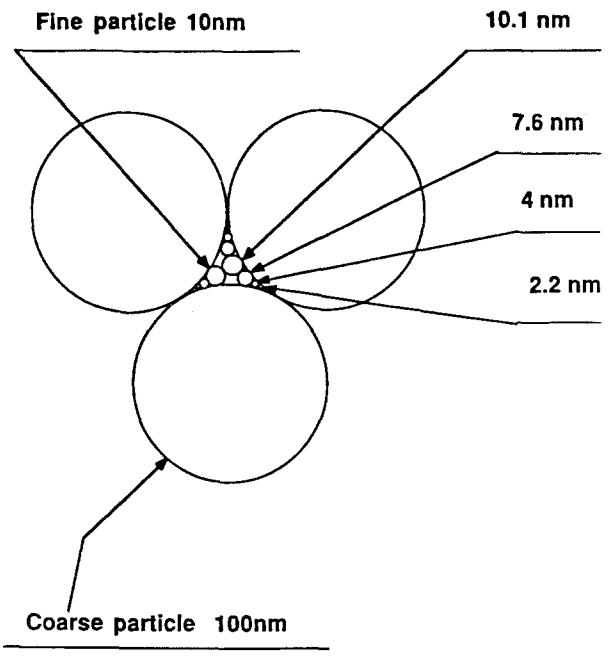

Figure 13 Two-dimensional simulation of triangular close packing of bimodal mixtures of 100 and 10 nm spheres.

considered that the small particles were 10 nm diameter. It can be seen that once a 10 nm particle is placed within the triangular pore, the possible pore radii are successively 10.1 and 7.6 nm. These values are quite close to the results obtained from the BET experiments (Fig. 7). Thus, it would seem that the model is close to the real situation. The type of packing in the cakes would be one of three contacting spheres (i.e., close packed), with one to two small particles in the pore. This is a situation which would promote a higher packing density, a smaller pore size and result in reduced permeability, as was observed experimentally.

The current model is limited to a two-dimensional case due to the fact that in the case of close packing, only two possibilities exist, i.e. "triangular" or "square" pores, and the model can easily be related to the experimental results of pore size and pore size distribution obtained by BET measurements. In addition, the BET measurements as well as the mercury porosimetry measurements are related to the cross-sectional area of the pores. For this reason, the experimental results may allow us to determine which one of the solutions would be closer to reality. It is evident that a three dimensional model would be preferable and more realistic; however, this type of simulation is quite complex. Moreover, a large number of solutions are theoretically possible and, in order to determine which one fits reality best, other types of experiments would be needed, such as small angle neutron scattering.

As was shown in Fig. 8, there is a rapid increase in density in the range 0–30 vol % fines and a slow decrease in density in the range 30–100 vol % fines. The density values calculated for the range 0–100 vol % fines show that the maximum density occurs at 30 vol % fines. This is in good agreement with the different studies on the packing of bimodal mixtures of hard spheres where the maximum in density occurs at ~ 30 vol % fines. It can also be noticed that the densities for 0 and 100 vol % fines cases are 64.2 and 64.3% theoretical, respectively. These are in good agreement with the packing densities reported in the literature for the "random close packing" of monosized hard spheres. There is a maximum density of 68.07% theoretical at 30 vol % fines. From the data on the packing of bimodal mixtures of hard spheres, the maximum in density is attained at 30 vol % fines with an experimental density of about 80% theoretical for a diameter ratio of 10. This difference in the values of the maximum density achieved could be due to several factors. First, in this study, the particles are in the sub-micrometre size range, which may give rise to some flocculation of the fine fraction or heteroflocculation of the fine and large fractions. In addition, the charged particle surfaces may lead to some deviation from the case of metal shot, i.e. the particles may have larger effective diameters due to double layer thickness and hydration layer.

Iler [23] showed that the solubility of amorphous silica varies as a function of pH. The solubility decreases from 150 p.p.m. to 100 p.p.m. in the pH range 2–7. At pH 7, the solubility is at a minimum of 100 p.p.m. However, the solubility increases dramatically in the pH range 7–10, going from 100 p.p.m. to 1000 p.p.m. The solubility of silica is higher when the silica surface is convex, and lower when it is concave. In fact, the smaller the radius of curvature, the greater the effect on solubility. Thus, because smaller particles have smaller positive radii, they have a higher equilibrium solubility. Therefore, the smaller particles may tend to dissolve, and the larger ones may tend to grow. In the case where the silica particles flocculate at the point of contact, the radius of the curvature between them is extremely small and negative. The silica may tend to dissolve from the particle surfaces and be deposited at the point of contact to minimize the negative radius of curvature, thus forming a neck between the particles. This evolution of contact zones between particles could explain why, even if one could distinguish spherical forms in the scanning electron micrographs in some areas, the particles did not seem separated from one another. This could also account for the presence of particles of about 50 nm in a cake with 100 vol % 10 nm particles.

5. Conclusions

Filtration experiments were carried out using a high pressure transparent casting cell on colloidal suspensions (at 30 wt %, ~ 16 vol %) with bimodal mixtures of 10 and 100 nm silica particles. The zeta potential measurements versus pH, indicated a zero point of charge at pH 2, and the density of those powders were 2.18–2.19 $g\,cm^{-3}$, in good agreement with reported values. The viscosity measurements showed a slightly shear-thickening behaviour. The viscosity increased when the diameter of the particles decreased, most

likely due to electroviscous effects. A minimum in viscosity was observed for bimodal mixtures at 30 vol % fines. During filtration, the thickness of the cakes follows a linear behaviour when plotted as a function of the square root of time. The permeability of such cakes initially decreases then increases slightly as the fraction of fines is increased. As the fraction of fines increases, the peak in the pore size distribution decreases from $\sim$ 15 nm to 4 nm diameter. The variation of packing density with fraction of fines follows the evolution reported by McGeary and others for bimodal mixtures of hard spheres [26–29]. In these experiments, the maximum measured density was 68.07% theoretical at 30 vol % fines. The packing densities obtained for both 0 and 100 vol % fines are close to the values reported in the literature for random close packing of hard spheres. A two-dimensional model of three close packed spheres fits the pore size data results obtained much better than a model of four contacting spheres.

Acknowledgements

The authors thank the Rutgers University Center for Ceramics Research for the financial support for this work. In addition, the discussions and insight provided by Dr K. Bridger, Dr S. Rao, and M. J. Smyth are also greatly appreciated.

References

1. F. L. KENNARD, in "Ceramic processing", Vol. 7 (1986) p. 1095.
2. J. A. MANGELS, *ibid.* Vol. 7 (1986) p. 1112.
3. F. F. LANGE, *J. Amer. Ceram. Soc.* **67** (1984) 83.
4. W. D. KINGERY and B. FRANCOIS, in "Sintering and related phenomena", edited by G. C. Kuczynske, N. A. Hooton, G. F. Gibbons (Gordon and Breach, NY, 1967) p. 471–98, .
5. R. M. CANNON, in "Oxidation of non-oxide ceramics" edited by T. E. M. Mitchell *et al.* (Case-Western Reserve University, report to Air Force Office of Scientific Research, Contract E-49620-78-C0053, June, 1981).
6. J. S. HAGGERTY, Energy Laboratory Report, MIT-EL 82-002, DARPA N00014-77-C-0581 (MIT, Cambridge, MA, 1982).
7. C. HERRING, *J. Appl. Phys.* **21** (1950) 301.
8. E. MATIJEVIC, *Acc. Chem. Res.* **14** (1981) 22.
9. W. STOBER, A. FINK, E. BOHN, *J. Colloidal Interface Sci.* **26** (1968) 62.
10. K. S. MAZDIYASNI, in "Proceedings of the Materials Research Society Symposia", 1984, Vol. 32, (Elsevier Science, New York 1984) p. 175.
11. E. A. BARRINGER and H. K. BOWEN, in "Proceedings of the International Institute for the Sciences of Sintering, Belgrade, Yugoslavia, 1983.
12. E. A. BARRINGER, R. BROOK, and H. K. BOWEN, in "Proceedings of the Sixth International Conference on Sintering and Related Phenomena, including Heterogeneous Catalysts", Notre Dame, Indiana, June, 1983.
13. E. A. BARRINGER and H. K. BOWEN, *Langmiur* **1** (1985) 414.
14. *Idem. ibid.* **1** (1985) 421.
15. B. FEGLEY, Jr., E. A. BARRINGER, and H. K. BOWEN, *J. Amer. Ceram. Soc.* (1984) C114.
16. E. A. BARRINGER, N. JUBB, B. FEGLEY, R. L. POBER, and H. K. BOWEN, in "Ultrastructure processing of ceramics, glasses, and composites", edited by L. L. Hench and D. R. Ulrich (Wiley, New York, 1984) p. 315.
17. W. R. CANNON, S. C. DANFORTH, J. H. FLINT, J. S. HAGGERTY, and R. A. MARRA, *J. Amer. Ceram. Soc.* **65** (1982) 324.
18. A. J. HURD, in "Proceedings of the Materials Research Society Symposia", Vol. 73 (Elsevier Science, New York, 1986) p. 345.
19. H. K. BOWEN, in "Proceedings of the Materials Research Society Symposia", Vol. 24 (Elsevier Science, New York, 1984) p. 1.
20. F. F. LANGE, *J. Amer. Ceram. Soc.* **72** (1989) 3.
21. J. E. RITTER, S. V. NAIR, P. GENNARI, W. A. DUNLAY, J. S. HAGGERTY, and G. J. GARVEY, *ibid.*
22. S. C. DANFORTH and J. S. HAGGERTY, *ibid.* **66** (1983) C58.
23. S. C. DANFORTH and M. H. RICHMAN, *Bull. Amer. Ceram. Soc.* **62** (4) (1983) 501.
24. I. A. AKSAY, in "Advances in ceramics", Vol. 9. "Forming of Ceramics", edited by J. A. Mangels (American Ceramic Society, Westerville, Ohio, 1984).
25. E. LINIGER, R. RAJ, *J. Amer. Ceram. Soc.* **70, 11** (1987), 843.
26. R. K. McGEARY, *ibid.* **44** (1961) 513.
27. C. C. FURNAS, *Ind. Engng Chem.* **23** (1931) 1052.
28. A. E. R. WESTMAN and H. R. HUGILL, *J. Amer. Ceram. Soc.* **13** (1930) 767.
29. H. E. WHITE and S. F. WALTON, *ibid.* **20** (1937) 155.
30. R. K. ILER, "The Chemistry of Silica" (Wiley, New York, 1979).
31. F. M. TILLER, C. S. YEH, C. D. TSAI, and W. CHEN, in "Proceedings of the Fourth World Filtration Congress", Ostend, Belgium, 19–25 April, 1986.
32. G. D. SCOTT, *Nature* **188** (1960) 908.

Received 14 February
and accepted 3 December 1990